

# Geophysical Research Letters<sup>®</sup>

## RESEARCH LETTER

10.1029/2022GL099053

### Key Points:

- We present a method for eikonal tomography with physics-informed neural networks
- We apply it to a dense seismic array in the northeastern Tibetan Plateau with good validation compared with traditional approaches
- Traveltime reconstruction inversion mitigates traveltime measurement error and the number of traveltime sets can be significantly reduced

### Supporting Information:

Supporting Information may be found in the online version of this article.

### Correspondence to:

S. A. L. de Ridder and Y. Chen,  
[s.deridder@leeds.ac.uk](mailto:s.deridder@leeds.ac.uk);  
[johnyc@sustech.edu.cn](mailto:johnyc@sustech.edu.cn)

### Citation:

Chen, Y., de Ridder, S. A. L., Rost, S., Guo, Z., Wu, X., & Chen, Y. (2022). Eikonal tomography with physics-informed neural networks: Rayleigh wave phase velocity in the northeastern margin of the Tibetan Plateau. *Geophysical Research Letters*, 49, e2022GL099053. <https://doi.org/10.1029/2022GL099053>

Received 12 APR 2022  
Accepted 19 OCT 2022

© 2022. The Authors.

This is an open access article under the terms of the [Creative Commons Attribution-NonCommercial-NoDerivs License](https://creativecommons.org/licenses/by-nc-nd/4.0/), which permits use and distribution in any medium, provided the original work is properly cited, the use is non-commercial and no modifications or adaptations are made.

## Eikonal Tomography With Physics-Informed Neural Networks: Rayleigh Wave Phase Velocity in the Northeastern Margin of the Tibetan Plateau

Yunpeng Chen<sup>1,2</sup> , Sjoerd A. L. de Ridder<sup>1</sup> , Sebastian Rost<sup>1</sup> , Zhen Guo<sup>2,3</sup> , Xiaoyang Wu<sup>2</sup>, and Yongshun Chen<sup>2,3</sup> 

<sup>1</sup>School of Earth and Environment, University of Leeds, Leeds, UK, <sup>2</sup>Department of Ocean Science and Engineering, Southern University of Science and Technology, Shenzhen, China, <sup>3</sup>Southern Marine Science and Engineering Guangdong Laboratory (Guangzhou), Guangzhou, China

**Abstract** We present a novel eikonal tomography approach using physics-informed neural networks (PINNs) for Rayleigh wave phase velocities based on the eikonal equation. The PINN eikonal tomography (pinnET) neural network utilizes deep neural networks as universal function approximators and extracts traveltimes and velocities of the medium during the optimization process. Whereas classical eikonal tomography uses a generic non-physics based interpolation and regularization step to reconstruct traveltime surfaces, optimizing the network parameters in pinnET means solving a physics constrained traveltime surface reconstruction inversion tackling measurement noise and satisfying physics. We demonstrate this approach by applying it to 25 s surface wave data from ChinArray II sampling the northeastern Tibetan plateau. We validate our results by comparing them to results from conventional eikonal tomography in the same area and find good agreement.

**Plain Language Summary** Eikonal tomography is an efficient approach to resolve velocity structure from surface wave data. Classical ambient noise eikonal tomography constrains the local phase velocity with all station pairs and uses a generic interpolation to reconstruct traveltime surfaces. Here we implement physics-informed neural networks for eikonal tomography. Unlike traditional neural networks that only rely on a large volume of data that is agnostic to physical laws, physics-informed neural network eikonal tomography (pinnET) can combine the data-driven model and theory-based model, which includes eikonal equation and boundary conditions as physical constraints on the system. We apply this pinnET to northeastern Tibetan plateau and our Rayleigh wave phase velocity results are quite similar with other established methods but use much less data.

## 1. Introduction

Eikonal tomography was proposed to directly obtain the phase velocity of surface waves from interpolated phase traveltime surfaces (Lin et al., 2009) and is often applied to ambient noise surface wave data. In ambient noise eikonal tomography, each station is considered as a “source” and the traveltime surface can be estimated between this source and other stations whose recordings have been cross-correlated with those of the main source. Eikonal tomography constrains the phase velocity by locally evaluating the eikonal equation. The eikonal equation is a first-order nonlinear partial differential equation (PDE) that represents a high frequency approximation to the wave equation (Shearer, 2019). The eikonal equation directly relates wave velocity and propagation directions to the spatial gradients of a traveltime surface (Lin & Ritzwoller, 2011). Following Lin et al. (2009), a series of new applications in eikonal tomography soon followed (i.e., De Ridder, 2011; De Ridder et al., 2015; Gouédard et al., 2012; Qiu et al., 2019).

In contrast to traditional surface wave tomography, eikonal tomography automatically accounts for ray bending and thereby provides a more accurate representation of wave propagation (Lin et al., 2009). However, classical eikonal tomography uses a generic interpolation algorithm to reconstruct the traveltime surfaces between stations in order to evaluate the eikonal equation that yields the velocity. This approach effectively biases the velocity depending on the particular algorithm used for interpolation. Linear interpolation enforces a homogeneous velocity between stations, whereas bicubic spline interpolation smoothens the traveltime surfaces reducing the resolution. One way to solve this problem is to introduce known physical constraints, similar to the introduction of the

wave equation as PDE constraint in seismic waveform fitting (De Ridder & Maddison, 2018; Shaiban et al., 2022; Van Leeuwen & Herrmann, 2013, 2015). Here we argue that a physics based interpolation is easily achieved using neural networks (NNs) by formulating the surface wave tomography problem in a physics-informed neural network (PINN) framework.

Over the past decade, deep learning has been used as an efficient tool in many domains, such as image recognition (Krizhevsky et al., 2012), natural language processing (LeCun et al., 2015) and object detection (Pathak et al., 2018). In seismology, deep learning also found many applications to improve seismic data processing and imaging (i.e., Lim, 2005; Liu et al., 2018; Zhang et al., 2014). Recently, an advanced deep learning framework, called PINN, was proposed to solve PDEs, which imposes deep neural networks (DNNs) as universal function approximators (Raissi et al., 2019). In contrast to classic DNNs, PINNs are better placed to combine data science and theory-based models. They leverage the mathematical descriptions of the physical process as constraints to the data driven deep learning approaches and determine the physical parameters during the training process. PINNs have successfully been included in other machine learning approaches, like transfer learning and meta-learning (Chakraborty, 2021; Psaros et al., 2021), probabilistic PINNs (Grigo & Koutsourelakis, 2019; L. Yang et al., 2021) and error analysis (Jiao et al., 2021; Mishra & Molinaro, 2020). This idea is highly beneficial to seismic tomography for avoiding the iterative process required by the nonlinearity and can directly extract the predicted parameters (e.g., velocity) for the model. The PINN framework has already shown great potential in solving the seismic forward problem (Moseley et al., 2020; Smith et al., 2020; Song et al., 2021; Waheed, Haghghat, et al., 2021) and seismic inverse problem (Song & Alkhalifah, 2021). Waheed, Alkhalifah, et al. (2021) suggested a PINN framework for exploration scale seismic tomography based on a factored eikonal equation, supported with synthetic examples.

Here we present a PINN-based algorithm for eikonal tomography and show the application in regional scale. The PINN framework is realized in SciAnn—a high-level deep learning library for physics-informed deep learning (Haghghat & Juanes, 2021). We use the eikonal equation to define the loss function, which is used to describe the difference between predicted and true value, and train this NN to obtain the solution of the inversion by minimizing the loss function. In contrast to traditional eikonal tomography, this approach utilizes DNNs to optimize the field data and extract the traveltime and velocity during the optimization process. We will first formulate PINN eikonal tomography (pinnET) and then present the results of a field data trial using data from ChinArray II in the NE Tibetan plateau, see Figure 2a.

## 2. Physics-Informed Deep Learning for Eikonal Tomography

A classical NN is defined as a mathematical operation (a general function) that generates an output value given several input values. Training data is used to optimize the parameters of the NN such that the error between predicted output and true output (in the training data) is minimized (here using an L2 loss function):

$$\mathcal{L}(\theta_\tau) = \sum_j^{N_{src}} \sum_i^{N_{rcv}} |N_\tau(\theta_\tau; \mathbf{x}_{r,i}, \mathbf{x}_{s,j}) - \tau_{i,j}|^2, \quad (1)$$

where  $i$  and  $j$  are the index of receivers and sources respectively,  $\theta_\tau$  are the hyperparameters of the traveltime NN  $N_\tau$ ,  $N_{src}$  represents the number of sources,  $N_{rcv}$  represents the number of receivers,  $\mathbf{x}_{r,i} = (x_r, y_r)_i$  and  $\mathbf{x}_{s,j} = (x_s, y_s)_j$  are the receiver and source locations of the spatial coordinates  $\mathbf{x}$ ,  $\tau_{i,j}$  represents the traveltime surfaces of seismic waves.  $\mathcal{L}$  is the loss function.

Representing traveltimes by NNs does not guarantee that their output conforms to the physics of wave propagation. We add a physics constraint to the NN (forming a PINN). In contrast to classical NNs, PINNs ensure interpretability in NNs by combining data sets and physical constraints (Figure 1). In this study, we choose the eikonal equation as the governing physical law. The eikonal equation directly relates the local phase velocity to the local spatial gradients of the traveltime surface. In the high frequency approximation, the eikonal equation can be expressed in first order-hyperbolic form (e.g., Wielandt, 1993):

$$|\nabla\tau(\mathbf{x})|^2 \approx \frac{1}{c^2(\mathbf{x})}, \quad (2)$$

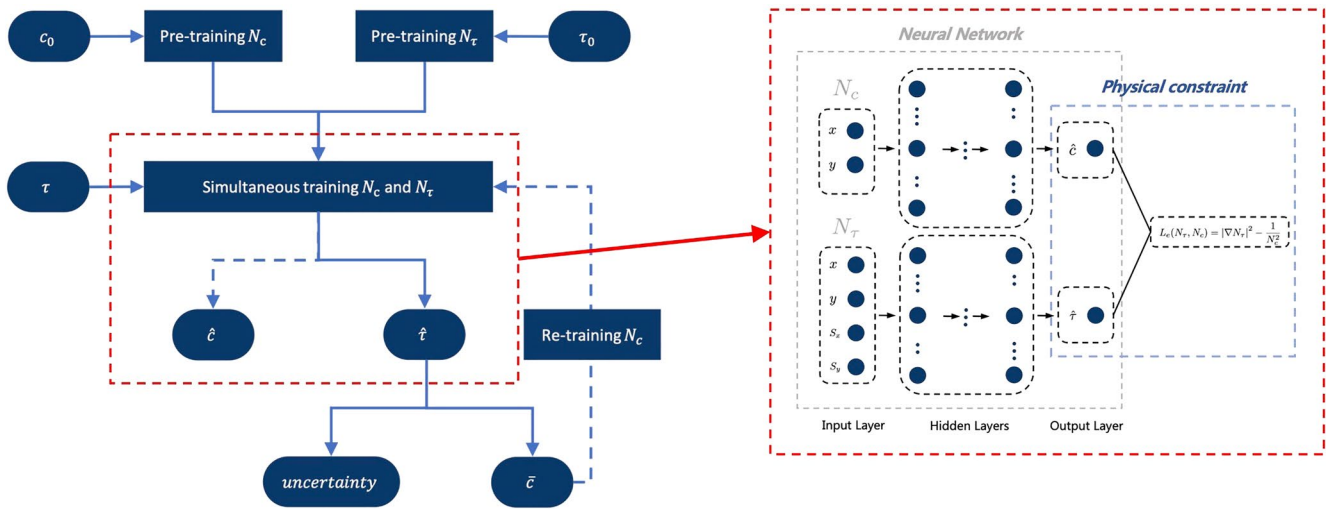


**Figure 1.** Workflow and PINN framework for traveltime eikonal tomography, where  $c_0$  and  $\tau_0$ : initial phase velocity and traveltime;  $N_c$  and  $N_\tau$ : neural networks of velocity and traveltime;  $\tau$ : observed traveltime;  $\hat{c}$  and  $\hat{\tau}$ : predicted phase velocity and traveltime from PINN eikonal tomography (pinNET);  $\bar{c}$ : average phase velocity from all sources. In the PINN algorithm, the loss function  $L$  consists of two parts: the neural networks composed of  $N_c$  and  $N_\tau$  used to minimize the misfit of the traveltime data providing the approximate solution and the physical constraint utilizing the approximate solution and adding the residual of physical equation. This physical constraint contains the eikonal equation and appropriate boundary conditions.

where  $\nabla$  is the Laplace operator. The traveltime is expressed as a continuous scalar function  $\tau(\mathbf{x})$ , and  $c(\mathbf{x})$  represents the local phase velocity on the surface of the Earth, at location  $\mathbf{x} = (x, y)$ . In our study, both the traveltimes and the phase velocity are expressed as outputs of a NN, thus the physical constraint can be written as:

$$L_e(N_\tau, N_c) = |\nabla N_\tau|^2 - \frac{1}{N_c^2}, \quad (3)$$

where  $N_\tau = N_\tau(\theta_\tau; \mathbf{x}_r, \mathbf{x}_s)$  is the traveltime at  $\mathbf{x}_r$  from a source at  $\mathbf{x}_s$ , and  $N_c = N_c(\theta_c; \mathbf{x}_r)$  is the phase velocity at  $\mathbf{x}_r$ , representing the traveltime surfaces  $\tau(\mathbf{x}_r, \mathbf{x}_s)$  and velocities  $c(\mathbf{x}_r)$ .  $\theta_\tau$  and  $\theta_c$  are hyperparameters of traveltime and velocity NNs, respectively. Combining Equations 1 and 3, we define the PINN loss function:

$$\mathcal{L}(\theta_\tau, \theta_c) = \sum_j^{N_{src}} \sum_i^{N_{rev}} \left[ |N_\tau(\theta_\tau; \mathbf{x}_{r,i}, \mathbf{x}_{s,j}) - \tau_{i,j}|^2 + \epsilon_e |L_e(N_\tau(\theta_\tau; \mathbf{x}_{r,i}, \mathbf{x}_{s,j}), N_c(\theta_c; \mathbf{x}_{r,i}))|^2 \right], \quad (4)$$

where  $\epsilon_e$  is a parameter that describes the relative weight of the eikonal constraint. Both terms of the loss function are evaluated at collocated points, coinciding with the observations locations of the traveltime data. If  $\epsilon_e$  is chosen too large, the first estimate for the velocity in the eikonal equation constraint will completely control the outcome of the optimization. In that regime, the velocity NN will not be updated, and the velocity captured in the outputs of the traveltime NN will not deviate from the first estimate for the velocity. Alternatively, if  $\epsilon_e$  is too small, the observed data will dominate this process and the results are evaluated without actually enforcing the physics constraint. So  $\epsilon_e$  was chosen to be in between these two regimes, which we ascertained through tests was a rather narrow range. SciAnn (Haghighat & Juanes, 2021) allows to specify physics constraints symbolically and handles them through automatic differentiation in the optimisation.

Here the training process is the only step needed to learn the correct physics. The training process aims to obtain the hyperparameters  $\hat{\theta}_\tau$  and  $\hat{\theta}_c$  by minimizing the loss function:

$$\arg \min_{\theta_\tau, \theta_c} \{\mathcal{L}(\theta_\tau, \theta_c)\} \rightarrow \hat{\theta}_\tau, \hat{\theta}_c. \quad (5)$$

In order to train a PINN, we would need the true velocity model of the Earth. The principle concept of pinNET is to update the velocity in the eikonal equation (physics) constraint, while training a NN that fits the observations.

We follow a training procedure that starts with individually pre-training the traveltime and velocity NNs using a starting velocity model, followed by iterated training in which the traveltime and velocity NNs may be updated

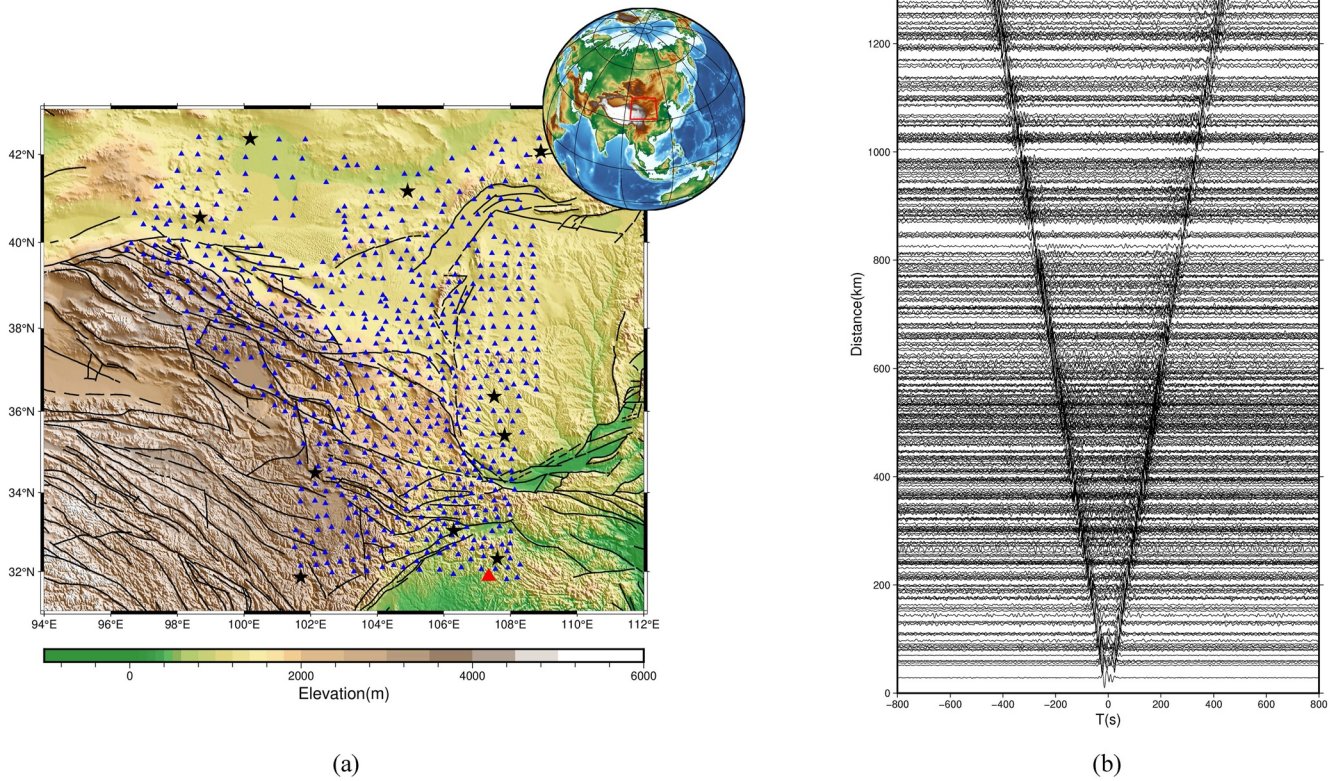


**Figure 2.** (a) Overview of the station network in Tibet used in data example. Black lines indicate main faults, blue triangles indicate stations of the network and black stars indicate the selected source stations for the velocity determination. (b) An example of Z-Z component cross-correlations for station pairs at station 51511 (red triangle in (a)), the V-shaped arrivals are Rayleigh waves.

simultaneously or sequentially (individually retraining the velocity NN), see Figure 1. The starting velocity  $c_0$ , for pre-training  $N_c$ , is calculated by dividing the sum of distances between all station pairs by the sum of observed traveltimes. The initial traveltimes  $\tau_0$ , for pre-training  $N_\tau$ , are calculated by dividing each distance between station pair by the initial velocity  $c_0$ . The traveltime NN is pre-trained using a loss function as in Equation 1, with  $\tau_{i,j} = \tau_{0,i,j}$  for pre-training, and the velocity NN is pre-trained using:

$$\mathcal{L}(\theta_c) = \sum_i^{N_{grid}} [|N_c(\theta_c; \mathbf{x}_i) - c_i|^2], \quad (6)$$

with  $c_i = c_{0,i}$  for pre-training, where  $N_{grid}$  is the number of grid points. The pre-training process provides good initial weights for the NNs and results in a stable convergence during the process of iterated training. Simultaneous training aims to minimize the loss function in Equation 4. After this process, the velocity can be extracted in two different ways. The first method is by evaluating the velocity directly from the trained NNs, denoted  $\hat{c}$ :

$$\hat{c}(\mathbf{x}) = N_c(\hat{\theta}_c; \mathbf{x}), \quad (7)$$

where  $\hat{c}$  is the trained velocities. The second method is by evaluating the traveltime NN on a fine regular grid using finite differences, yielding  $\bar{c}$ :

$$\bar{c}(\mathbf{x}) = \frac{1}{N_{src}} \sum_j^{N_{src}} \left| \frac{1}{\nabla N_\tau(\hat{\theta}_\tau; \mathbf{x}, \mathbf{x}_{s,j})} \right|, \quad (8)$$

where  $\bar{c}$  is the average velocity surfaces from all predicted traveltimes,  $N_{\hat{c}}$  indicates the trained traveltimes surfaces  $\hat{c}$ . In fact we employ a trimmed geometric mean (discarding the 10 percentile outliers at both extremes) and compute its corresponding standard deviation. The second method is relevant for sequential updates during which the velocity NN is updated explicitly by minimizing the loss function in Equation 6. We perform 2 outer iterations (with one sequential updating) to update the estimate for the velocity, and find that this strategy accelerates the overall convergence rate (see Supporting Information Figure S1). Another advantage of using traveltimes surfaces to predict the velocity is that it works robustly (parameter tuning is less tenuous) and comes with a measure of uncertainty (Figure 4c).

### 3. PINNs Eikonal Tomography on Northeastern (NE) Tibetan Plateau

To demonstrate the suitability of our algorithm we apply it to a sample data set of 25 s period Rayleigh wave traveltimes collected from station of the ChinArray II network located on the NE Tibetan Plateau (Figure 2a). This data set allows us to compare the pinnET approach with other eikonal tomography solutions, traditional surface wave tomography and ambient noise surface wave tomography results. The station distribution of the network is also well suited for our approach and the tectonic history of the region shows a variety of structures which allow us to test the resolution capabilities of our pinnET approach.

Since the collision of the Indian and Eurasian continents (~60 Ma), the Tibetan Plateau was elevated due to the N-S shortening of the crust (Yin & Harrison, 2000). The physical processes that controlled the deformation and the mechanisms of crustal shortening remain subject for debate (i.e., Avouac & Tapponnier, 1993; Clark & Royden, 2000; England & Molnar, 1997; Guo & Chen, 2017; Hao et al., 2021; Tapponnier et al., 2001; Y. Yang et al., 2012). The ChinArray II data set has also been used to derive two-station Rayleigh wave tomography (Li et al., 2017), joint receiver functions and Rayleigh wave tomography (X. Wang et al., 2017), beamforming Rayleigh wave tomography (K. Wang et al., 2020) and Rayleigh wave eikonal tomography (Hao et al., 2021) allowing us to compare our results with more established methods. The traveltimes data at each source station are obtained based on the seismic ambient noise cross-correlations between all station pairs and arrival time picking. Here we choose Rayleigh wave data at 25 s period as a proof-of-concept data set to reveal phase velocity structure beneath NE Tibetan Plateau. In contrast to standard ambient noise or eikonal tomography we restrict the number of sources used in our approach to 10 sources recorded at all 676 stations of the network compared to all source-receiver combinations common in other methods. We randomly choose 10 sources to provide a good coverage of the model space. The training points are selected as the cross-correlated traveltimes between those and other stations but we removed the points 1 km around the sources to avoid singularity around them. The physics constraint is only enforced at the spatial locations of all the training traveltimes data.

Our PINNs algorithm for traveltimes eikonal tomography comprises two parts: the traveltimes NN that is used to approximate the traveltimes  $\hat{t}_{s_i}$  and the velocity NN which aims to extract the velocity  $\hat{c}(\mathbf{x})$ . There are 10 hidden layers in both NN, but for the traveltimes NN, each layer contains 20 neurons while only 5 neurons in each layer of velocity NNs. The size and numbers of layers in the NN were tuned to be able to represent all 10 traveltimes surfaces with sufficient accuracy as not to reduce uncertainty in the final velocity. The “*arctan*” function is used as the activation function for the hidden layers. The optimizer is defined as the “*adam*” optimizer (Kingma & Ba, 2014), which is computationally efficient and widely used in deep learning. We divide all samples into a batch size of 676 and train the networks for 2,000 epochs. The learning rate for all samples is 0.0002. These hyperparameters were all chosen based on systematic synthetic tests.

We use checkerboard tests to evaluate the resolution of our results (Figure 3). The synthetic velocity model has a background velocity of 3.45 km/s on  $8 \times 8$  anomalies. The magnitudes of the velocity perturbations are 2% and these anomalies have a maximum radius of 75 km distributed in the latitude and longitude direction, respectively. The distance between alternating low and high velocity anomalies is therefore 150 km (Figure 3a). We choose the same number and distribution of 676 stations with 10 sources (Figure 2a) for the checkerboard resolution tests as in the recorded data. Gaussian noise with a mean of 0.1 s and a standard deviation of 0.01 has been added to the traveltimes data to simulate noise in the observed data. Figure 3b shows the recovered velocity structure by PINNs eikonal tomography. Most anomalies can be well recovered when the ray coverage is sufficient. Less well sampled structure at the edge of station networks is still acceptably resolved. We observe some lateral smearing especially in SW-NE direction in the north of the network which could be related to the choice of the source distribution. The checkerboard tests show that our phase velocity results are reliable with these parameters at 25 s.

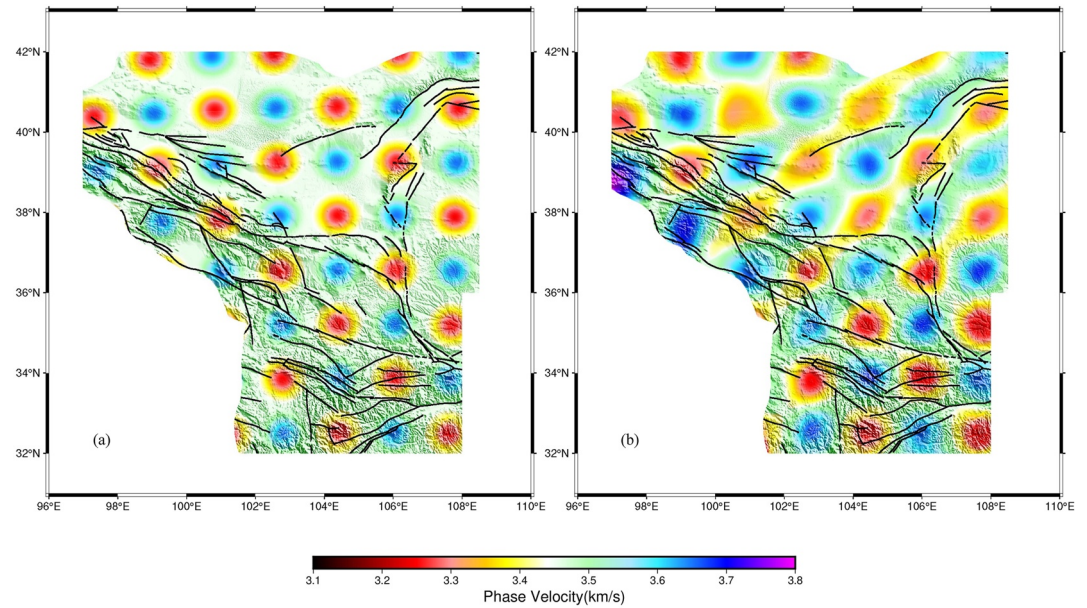


**Figure 3.** (a) Input synthetic velocity model of checkerboard resolution test for pinnET; (b) Retrieved Rayleigh wave phase velocity at periods of 25 s.

We apply our pinnET approach to recorded ambient noise data from the Tibetan Plateau (Figure 2a). The convergence rate of the different training processes is shown by the loss curves in Figure S1 in Supporting Information. Using 10 sources to all stations and averaging the velocities from the solution for different sources (Equation 8), we resolve the phase velocity structure (Figure 4a) beneath NE Tibetan Plateau. Comparing with solutions derived from other Rayleigh wave tomography approaches, we find very good agreement. We show a direct comparison with the results at 25 s by ambient noise eikonal tomography. The phase velocities we find in the region are within  $\pm 0.1$  km/s of other methods. We find good agreement with the lower velocities beneath the Songpan-Ganzi block, Qilian and Western Qinling Orogen. At the southeastern and northwestern edges of the network we find lower velocities beneath the Sichuan Basin and the Central Asian Orogenic Belt. This could be because bicubic spline interpolation (used in conventional eikonal tomography) flattens the interpolated travel-time surfaces near the edges of the data coverage. Boundaries of all features are in good agreement with other studies (Zhong et al., 2017; K. Wang et al., 2020). Figure 4c shows the Rayleigh wave local phase velocity uncertainty. The uncertainty of most area across the map is less than 0.02 km/s. Large uncertainties occur in a small part of the southeastern Ordos Block, the western Songpan-Ganzi Block and the eastern Sichuan basin, these are most likely due to data coverage in the random selection of 10 sources.

The observed difference between the phase velocity maps resulting from conventional eikonal tomography result and pinnET could be considered significant (in some areas in the order of 100 m/s). The resolution of pinnET (in general) depends on the observation station spacing, the trade off between the measurement errors in the data and the number of traveltimes sets (source instances) used, and on the hyperparameters of the NN, and parameters controlling the training process. The method is certainly memory efficient because compressing the traveltimes as outputs to a NN is a concept akin to compressed sensing. We use much less data to achieve the similar imaging with a benefit of including the physics constraint while reconstructing the traveltimes surfaces.

We restricted ourselves to an inversion at 25 s period. Data at other periods can be inverted using pinnET in the same way leading to wide spectrum phase velocity maps that can be inverted from surface wave tomography using traditional approaches or neural networks.

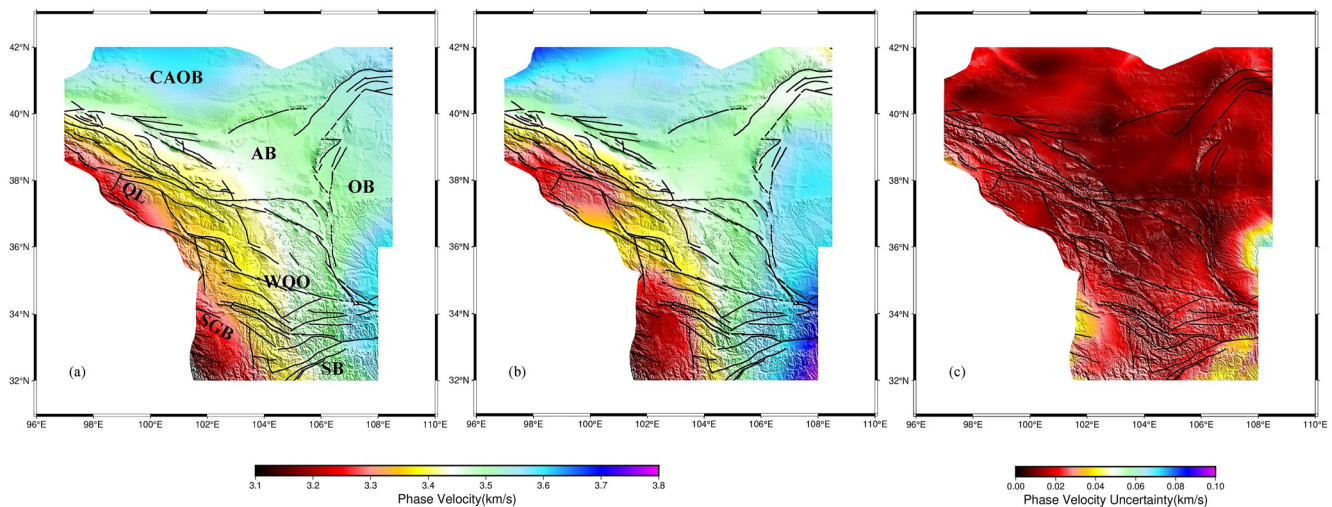


**Figure 4.** (a) The predicted 25s phase velocity map beneath NE Tibetan Plateau using PINN eikonal tomography (pinnET) (Block and structure are as follows: AB = Alxa Block; CAOB = Central Asian Orogenic Belt; OB = Ordos Block; QL = Qilian; SB = Sichuan basin; SGB = Songpan-Ganzi Block; WQO = Western Qinling Orogen); (b) The 25s phase velocity structure generated by conventional eikonal tomography; (c) The 25s phase velocity uncertainty map.

#### 4. Conclusions

We present a novel method for traveltimes eikonal tomography using PINNs and apply it to recorded field data. The method leverages neural networks as universal function approximators and utilizes the estimated medium properties in the eikonal equation which are treated as underlying physical laws. Reconstruction inversions based on NN function approximators are memory efficient. The hyperparameters of the NNs should be carefully selected to ensure the appropriate resolution of pinnET, for example, through a checkerboard test. The final algorithm is an eikonal tomography that uses physics consistent interpolation while reconstructing (interpolating) the traveltimes. The reconstruction inversion mitigates errors in the original traveltimes measurements and the number of traveltimes sets used in the training can be significantly reduced.

We applied the PINNs eikonal tomography on seismic data recorded by ChinArray II installed over the NE Tibetan Plateau. We extracted Rayleigh wave phase velocities at 25 s and associated uncertainties using only 10 sources. The results compares well to the velocity structure obtained by the conventional eikonal tomography using all 676 sources of the seismic networks.

#### Data Availability Statement

The traveltimes data sets used in this study and the Rayleigh wave phase velocity models can be downloaded at <https://doi.org/10.5281/zenodo.7223219>.

#### References

- Avouac, J.-P., & Tapponnier, P. (1993). Kinematic model of active deformation in central Asia. *Geophysical Research Letters*, 20(10), 895–898. <https://doi.org/10.1029/93gl00128>
- Chakraborty, S. (2021). Transfer learning based multi-fidelity physics informed deep neural network. *Journal of Computational Physics*, 426, 109942. <https://doi.org/10.1016/j.jcp.2020.109942>
- Clark, M. K., & Royden, L. H. (2000). Topographic ooze: Building the eastern margin of Tibet by lower crustal flow. *Geology*, 28(8), 703–706. [https://doi.org/10.1130/0091-7613\(2000\)028<0703:toftem>2.3.co;2](https://doi.org/10.1130/0091-7613(2000)028<0703:toftem>2.3.co;2)
- De Ridder, S. (2011). Ambient seismic noise tomography for exploration seismology at Valhall. In *AGU Fall Meeting Abstracts* (Vol. 2011, p. S31F-04).
- De Ridder, S., Biondi, B., & Nichols, D. (2015). Elliptical-anisotropic eikonal phase velocity tomography. *Geophysical Research Letters*, 42(3), 758–764. <https://doi.org/10.1002/2014gl062805>
- De Ridder, S., & Maddison, J. (2018). Full wavefield inversion of ambient seismic noise. *Geophysical Journal International*, 215(2), 1215–1230. <https://doi.org/10.1093/gji/ggy328>
- England, P., & Molnar, P. (1997). Active deformation of Asia: From kinematics to dynamics. *Science*, 278(5338), 647–650. <https://doi.org/10.1126/science.278.5338.647>

#### Acknowledgments

The authors acknowledge China Seismic Array Data Management Center at Institute of Geophysics, China Earthquake Administration for providing ambient noise data used in this study. The authors thank all the people who participated in the field deployment of seismic arrays for the ChinArray II project. This work is supported by the National Science Foundation of China (Grants 41890814 and U1901602). Y.P. C. is also supported by a split-site PhD program of SUSTech and the University of Leeds. Z.G. is also supported by Key Special Project for Introduced Talents Team of the Southern Marine Science and Engineering Guangdong Laboratory (Guangzhou) (GML2019ZD0210).

- Gouédard, P., Yao, H., Ernst, F., & van der Hilst, R. D. (2012). Surface wave eikonal tomography in heterogeneous media using exploration data. *Geophysical Journal International*, 191(2), 781–788. <https://doi.org/10.1111/j.1365-246x.2012.05652.x>
- Grigo, C., & Koutsourelakis, P.-S. (2019). A physics-aware, probabilistic machine learning framework for coarse-graining high-dimensional systems in the Small Data regime. *Journal of Computational Physics*, 397, 108842. <https://doi.org/10.1016/j.jcp.2019.05.053>
- Guo, Z., & Chen, Y. J. (2017). Mountain building at northeastern boundary of Tibetan Plateau and craton reworking at Ordos block from joint inversion of ambient noise tomography and receiver functions. *Earth and Planetary Science Letters*, 463, 232–242. <https://doi.org/10.1016/j.epsl.2017.01.026>
- Haghighat, E., & Juanes, R. (2021). Sciann: Akeras/tensorflow wrapper for scientific computations and physics-informed deep learning using artificial neural networks. *Computer Methods in Applied Mechanics and Engineering*, 373, 113552. <https://doi.org/10.1016/j.cma.2020.113552>
- Hao, S., Huang, Z., Han, C., Wang, L., Xu, M., Mi, N., & Yu, D. (2021). Layered crustal azimuthal anisotropy beneath the northeastern Tibetan Plateau revealed by Rayleigh-wave Eikonal tomography. *Earth and Planetary Science Letters*, 563, 116891. <https://doi.org/10.1016/j.epsl.2021.116891>
- Jiao, Y., Lai, Y., Lo, Y., Wang, Y., & Yang, Y. (2021). Error analysis of deep Ritz methods for elliptic equations. arXiv:2107.14478.
- Kingma, D. P., & Ba, J. (2014). Adam: A method for stochastic optimization. arXiv:1412.6980.
- Krizhevsky, A., Sutskever, I., & Hinton, G. E. (2012). Imagenet classification with deep convolutional neural networks. *Advances in Neural Information Processing Systems*, 25, 1097–1105.
- LeCun, Y., Bengio, Y., & Hinton, G. (2015). Deep learning. *Nature*, 521(7553), 436–444. <https://doi.org/10.1038/nature14539>
- Li, Y., Pan, J., Wu, Q., & Ding, Z. (2017). Lithospheric structure beneath the northeastern Tibetan Plateau and the Western Sino-Korea Craton revealed by Rayleigh wave tomography. *Geophysical Journal International*, 210(2), 570–584. <https://doi.org/10.1093/gji/ggx181>
- Lim, J.-S. (2005). Reservoir properties determination using fuzzy logic and neural networks from well data in offshore Korea. *Journal of Petroleum Science and Engineering*, 49(3–4), 182–192. <https://doi.org/10.1016/j.petrol.2005.05.005>
- Lin, F.-C., & Ritzwoller, M. H. (2011). Helmholtz surface wave tomography for isotropic and azimuthally anisotropic structure. *Geophysical Journal International*, 186(3), 1104–1120. <https://doi.org/10.1111/j.1365-246x.2011.05070.x>
- Lin, F.-C., Ritzwoller, M. H., & Snieder, R. (2009). Eikonal tomography: Surface wave tomography by phase front tracking across a regional broad-band seismic array. *Geophysical Journal International*, 177(3), 1091–1110. <https://doi.org/10.1111/j.1365-246x.2009.04105.x>
- Liu, D., Wang, W., Chen, W., Wang, X., Zhou, Y., & Shi, Z. (2018). Random noise suppression in seismic data: What can deep learning do? In *SEG Technical Program Expanded Abstracts 2018* (pp. 2016–2020). Society of Exploration Geophysicists.
- Mishra, S., & Molinaro, R. (2020). Estimates on the generalization error of Physics Informed Neural Networks (PINNs) for approximating a class of inverse problems for PDEs. arXiv:2007.01138.
- Moseley, B., Markham, A., & Nissen-Meyer, T. (2020). Solving the wave equation with physics-informed deep learning. arXiv:2006.11894.
- Pathak, A. R., Pandey, M., & Rautaray, S. (2018). Application of deep learning for object detection. *Procedia Computer Science*, 132, 1706–1717. <https://doi.org/10.1016/j.procs.2018.05.144>
- Psaros, A. F., Kawaguchi, K., & Karniadakis, G. E. (2021). Meta-learning PINN loss functions. arXiv:2107.05544.
- Qiu, H., Lin, F.-C., & Ben-Zion, Y. (2019). Eikonal tomography of the Southern California plate boundary region. *Journal of Geophysical Research: Solid Earth*, 124(9), 9755–9779. <https://doi.org/10.1029/2019jb017806>
- Raissi, M., Perdikaris, P., & Karniadakis, G. E. (2019). Physics-informed neural networks: A deep learning framework for solving forward and inverse problems involving nonlinear partial differential equations. *Journal of Computational Physics*, 378, 686–707. <https://doi.org/10.1016/j.jcp.2018.10.045>
- Shaiban, A., De Ridder, S., & Curtis, A. (2022). Wavefield reconstruction and wave equation inversion for seismic surface waves. *Geophysical Journal International*, 229(3), 1870–1880. <https://doi.org/10.1093/gji/ggac031>
- Shearer, P. M. (2019). *Introduction to seismology*. Cambridge university press.
- Smith, J. D., Azizadenehsheli, K., & Ross, Z. E. (2020). Eikonet: Solving the eikonal equation with deep neural networks. *IEEE Transactions on Geoscience and Remote Sensing*, 59(12), 10685–10696. <https://doi.org/10.1109/tgrs.2020.3039165>
- Song, C., Alkhalifah, T., & Waheed, U. B. (2021). Solving the frequency-domain acoustic VTI wave equation using physics-informed neural networks. *Geophysical Journal International*, 225(2), 846–859. <https://doi.org/10.1093/gji/ggab010>
- Song, C., & Alkhalifah, T. A. (2021). Wavefield reconstruction inversion via physics-informed neural networks. *IEEE Transactions on Geoscience and Remote Sensing*, 60, 1–12. <https://doi.org/10.1109/tgrs.2021.3123122>
- Tapponnier, P., Zhiqin, X., Roger, F., Meyer, B., Arnaud, N., Wittlinger, G., & Jingsui, Y. (2001). Oblique stepwise rise and growth of the Tibet Plateau. *Science*, 294(5547), 1671–1677. <https://doi.org/10.1126/science.105978>
- Van Leeuwen, T., & Herrmann, F. J. (2013). Mitigating local minima in full-waveform inversion by expanding the search space. *Geophysical Journal International*, 195(1), 661–667. <https://doi.org/10.1093/gji/ggt258>
- Van Leeuwen, T., & Herrmann, F. J. (2015). A penalty method for PDE-constrained optimization in inverse problems. *Inverse Problems*, 32(1), 015007. <https://doi.org/10.1088/0266-5611/32/1/015007>
- Waheed, U. B., Alkhalifah, T., Haghighat, E., Song, C., & Virieux, J. (2021). Pinntomo: Seismic tomography using physics-informed neural networks. arXiv:2104.01588.
- Waheed, U. B., Haghighat, E., Alkhalifah, T., Song, C., & Hao, Q. (2021). Pinneik: Eikonal solution using physics-informed neural networks. *Computers & Geosciences*, 155, 104833. <https://doi.org/10.1016/j.cageo.2021.104833>
- Wang, K., Lu, L., Maupin, V., Ding, Z., Zheng, C., & Zhong, S. (2020). Surface wave tomography of northeastern Tibetan Plateau using beamforming of seismic noise at a dense array. *Journal of Geophysical Research: Solid Earth*, 125(4), e2019JB018416. <https://doi.org/10.1029/2019jb018416>
- Wang, X., Li, Y., Ding, Z., Zhu, L., Wang, C., Bao, X., & Wu, Y. (2017). Three-dimensional lithospheric S wave velocity model of the NE Tibetan plateau and Western north China craton. *Journal of Geophysical Research: Solid Earth*, 122(8), 6703–6720. <https://doi.org/10.1002/2017jb014203>
- Wielandt, E. (1993). Propagation and structural interpretation of non-plane waves. *Geophysical Journal International*, 113(1), 45–53. <https://doi.org/10.1111/j.1365-246x.1993.tb02527.x>
- Yang, L., Meng, X., & Karniadakis, G. E. (2021). B-PINNs: Bayesian physics-informed neural networks for forward and inverse PDE problems with noisy data. *Journal of Computational Physics*, 425, 109913. <https://doi.org/10.1016/j.jcp.2020.109913>
- Yang, Y., Ritzwoller, M. H., Zheng, Y., Shen, W., Levshin, A. L., & Xie, Z. (2012). A synoptic view of the distribution and connectivity of the mid-crustal low velocity zone beneath Tibet. *Journal of Geophysical Research*, 117(B4). <https://doi.org/10.1029/2011jb008810>

- Yin, A., & Harrison, T. M. (2000). Geologic evolution of the Himalayan-Tibetan orogen. *Annual Review of Earth and Planetary Sciences*, 28(1), 211–280. <https://doi.org/10.1146/annurev.earth.28.1.211>
- Zhang, C., Frogner, C., Araya-Polo, M., & Hohl, D. (2014). Machine-learning based automated fault detection in seismic traces. In *76th EAGE Conference and Exhibition 2014* (Vol. 2014, pp. 1–5).
- Zhong, S.-J., Wu, J.-P., Fang, L.-H., Wang, W.-L., Fan, L.-P., & Wang, H.-F. (2017). Surface wave Eikonal tomography in and around the north-eastern margin of the Tibetan plateau. *Chinese Journal of Geophysics*, 60(6), 2304–2314.